T.3: Experimental studies and parametric investigation on laser directed energy deposition based additive manufacturing of Hastelloy-X thin walls and bulk structures

A. N. Jinoop
Laser Technology Division
Email: anjinoop@gmail.com

Abstract
Laser Directed Energy Deposition (LDED) is one of the advanced manufacturing technologies for building near-net-shaped engineering components in a layer-by-layer fashion using high power lasers as an energy source. Hastelloy-X (Hast-X) is one of the prominent nickel-based superalloys suitable for high-temperature applications due to its appropriate blend of high-temperature strength, toughness, and resistance to degradation in a corrosive or oxidizing environment. This work aimed to investigate the effect of key process parameters on the single-track deposition to identify the process window. Further, the identified process window has been used for building thin-wall structures and bulk structures. The acquired know-how has been used to correlate the effect of the process on the various properties including geometrical characteristics, microstructure formation and mechanical behaviour. The study has also been extended to understand the effect of in-situ and ex-situ treatments on the behaviour of the built structures. Finally, a process methodology has been developed to build a prototype printed circuit heat exchanger (PCHE) using LDED. These studies will fill the gap for an immediate need of the additive manufacturing community through a systematic acquisition of know-how on the processing and properties of LDED built Hast-X.

1. Introduction

Additive manufacturing (AM) is a "process of joining materials to make parts from 3D model data, usually layer upon layer, as opposed to subtractive manufacturing and formative manufacturing methodologies" [1]. As metals are most used material in the industries, AM evolved to build metallic components by transforming itself from a process for "design validation and prototyping" to a process for building "near-net shaped components" [2]. Being the tool of power and precision, lasers are also used for these applications and laser-based AM process is called Laser Additive Manufacturing (LAM). It provides freedom of shape design, material design, post-processing, and logistics, which attracts its deployment in several sectors including aerospace, power, medical and automotive, with rising demand in aerospace [3] and power sector [4] to build high-performance components subjected to extreme duty conditions. These extreme duty conditions require the materials with high strength, oxidation resistance and corrosion resistance at elevated temperatures [5], for which nickel-based superalloys are preferred choice. Hastelloy-X (Hast-X) is one of the nickel-based superalloys suitable for high-temperature applications due to its excellent blend of high-temperature strength, toughness, and resistance to degradation in a corrosive or oxidizing environment. The application of Hast-X includes components for various advanced power generation cycles like supercritical cycles and concentrated solar power plants [6], combustion zone components such as transition ducts, combustor cans, spray bars and flame holders in gas turbine engines [6], and intermediate heat exchanger for high temperature reactor applications [7]. Some of these applications use advanced designs and materials for improved performance, which can not be built using conventional manufacturing processes due to inherent process limitations. These limitations motivated to take up an assignment in this direction and the present work is focused on investigation and employment of the versatile LDED based LAM technique to deposit defect free Hast-X for building thin-wall and bulk structures and investigate their behavior at different process and service conditions.

The literature review indicates that only some of the nickel-based superalloys are explored by LDED. Significant amount of work on nickel-based superalloys are carried out on the processing of Inconel 718 [8-10] and Inconel 625 [11-13], with little work carried out on Inconel 100 [14], Inconel 690 [15], Inconel 738 [16], Rene [17] and Waspaloy [18] using LDED. The literature indicates that the material specific LDED processing strategies and parameters are essential for defect free deposition and the mechanical properties are a function of processing strategies, parameters, and the resultant microstructure [19]. In case of Hast-X, the major challenge in the processing is its susceptibility to hot cracking or solidification cracking. The solidification cracking temperature range (SCTR) of Hast-X is 190 °C, which indicates that the material has moderate to high crack susceptibility [20]. Based on the extensive literature survey, the following gap areas are identified:

(a) There is limited published literature on LDED of Hastelloy grade materials, like Hast-X, which shows a knowledge gap especially on the effect of process parameters on the track geometry and track quality for defect free deposition using LDED.

(b) LDED built thin-wall structures (multi-layer deposition) are basic blocks for building complex engineering components and thus, it is necessary to understand the characteristics of thin walls. There is a lack of comprehensive studies on the effect of process parameters and interlayer delay conditions on the geometry, microstructure and mechanical properties of LDED built nickel-based superalloy wall structures.

(c) Bulk structures (multiple overlapped tracks and multi-layer deposition) are necessary to build complex shaped engineering components with higher build rate. Literature shows the studies on the microstructure and mechanical properties of fusion welded and Laser Powder Bed Fusion (LPBF) processed Hast-X [21-23]. However, there is no literature available on the microstructure and mechanical properties of LDED built Hast-X bulk structures.

(d) LDED built bulk structures are generally subjected to several in-situ and ex-situ treatments for defect rectification and tailoring its properties [19]. In-situ sequential layer-by-layer laser re-melting (SLLR) can be deployed for reducing

the porosity, grain refinement and improving surface finish of LDED built components. Hast-X, being a solid solution strengthened superalloy, requires probing into the microstructural and mechanical characteristics of LDED built Hast-X in solution treated condition. There is no study available in open literature on the effect of in-situ SLLR and solution treatment on the behavior of LDED built Hast-X components.

(e) Literature confirms the suitability of Hast-X for building printed circuit heat exchangers (PCHE) [7]. However, there is no study available in public domain on the development of an LDED methodology using wall and bulk structures as basic blocks for realization of Hast-X heat exchanger.

In view of the above, there is a strong need for in-depth scientific understanding and detailed investigations on the processing, analysis of microstructure and mechanical properties of LDED built Hast-X wall and bulk structures at different process conditions.

2. Experimental details

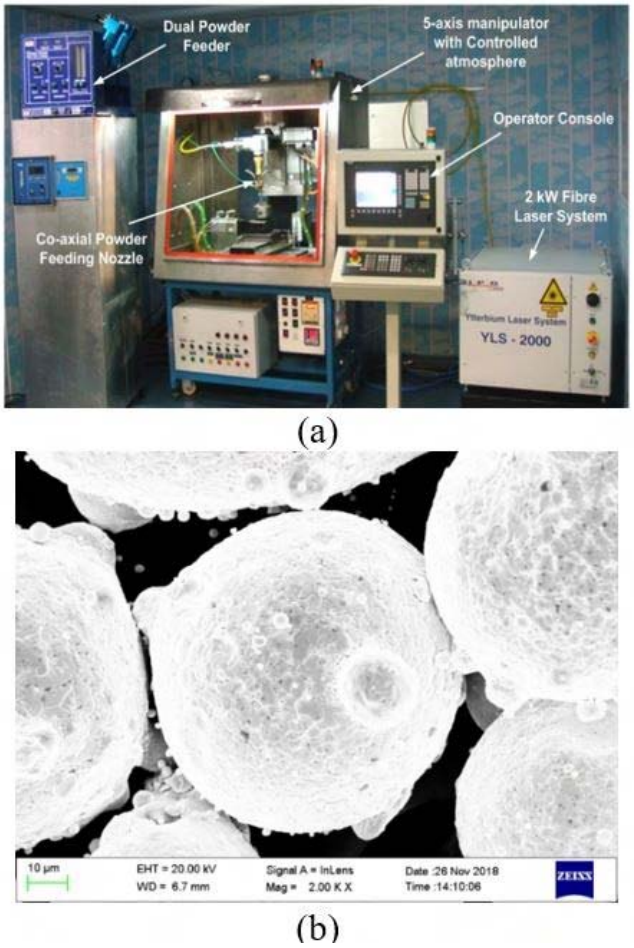

Fig. T.3.1: (a) System used for LDED of Hast-X and (b) powder morphology.

In the present work, an in-house developed 2 kW fiber laser based LDED system has been used for the deposition as shown in Figure T.3.1(a). The system consists of a 5-axis workstation inside a glove box, dual hopper powder feeder, and a co-axial nozzle. As the commercially available Hast-X powder has been used in the investigation, it was first characterized for morphology and chemical composition to confirm the quality and suitability for LDED deposition. It is observed that the powder is spherical in shape with fine satellites attached to it (Figure T.3.1(b)). The composition of the Hast-X powder is found to be within the nominal composition of Hast-X alloy [23].

3. Results and discussion

3.1 LDED built Hast-X single tracks

The geometry of LDED built Hast-X single tracks are analyzed using analytical modelling and verified by experimental analysis. In general, the geometry of the single track is a function of the LDED process parameters and the major LDED process parameters governing the single-track characteristics are laser power, scan speed and powder feed rate at a particular laser beam diameter. An analytical model is developed to predict the track geometry. The temperature distribution due to a continuous heat source, i.e., a Gaussian laser source can be calculated by considering a number of point sources. The Gaussian laser distribution is discretized into five different point heat sources and energy available at each point source is selected as per the Gaussian distribution. Track width is predicted by estimating the limit of the melt-pool to the substrate melting point by calculating the temperature distribution, while track height is estimated by using a combination of excess enthalpy and mass-balance approach. A comparison between experimental and modelling results exhibits a good agreement. It is observed that the maximum deviation in track width and track height are 12% and 18%, respectively. Experimental analysis shows that the track width and track height increases with an increase in laser power, reduction in scan speed and increase in powder feed rate. However, it is observed that the track width is highly influenced by the laser power, while the effect of powder feed rate is more significant on track height. It is also observed that the track aspect ratio (ratio of track width to track height) increases with an increase in laser power and scan speed; and decreases with an increase in the powder feed rate.

Investigations on the process window identification show that deposits are irregular at laser energy per unit powder feed (LEPF) of 4.5 kJ/g and 7.2 kJ/g, while cracked deposits are observed at higher LEPF of 19.2 kJ/g. Uniform deposits without cracks are observed for moderate LEPF in the range of 8.25 kJ/g to 13.2 kJ/g at all scan speeds (0.3 m/min to 0.7 m/min).

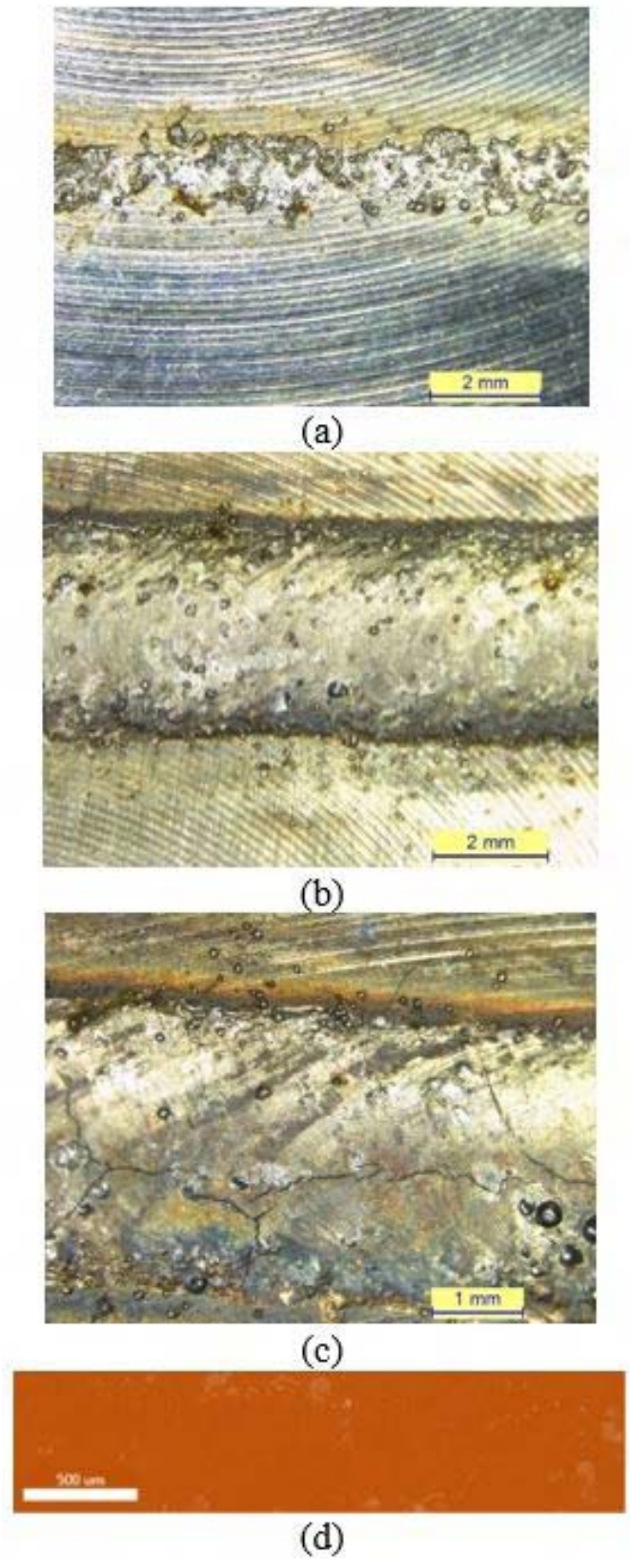

Fig. T.3.2(a): Single track morphology- (a) discontinuous, (b) continuous, (c) cracked and (d) Si segregation along crack.

When the LEPF is lower than 4.5 kJ/g, the requisite amount of energy for continuous deposition of material is not available, which yielded an irregular deposition. Figures T.3.2(a), T.3.2(b) and T.3.2(c) present the surface morphology of the discontinuous, continuous and cracked deposits, respectively. The cracking at higher LEPF can be due to a combination of higher thermal stresses in the solidifying deposit caused by large thermal strain and elemental segregations. Elemental mapping of the crack by scanning electron microscopy - energy dispersive spectroscopy (SEM-EDS) confirms the segregation of carbon and silicon (Figure T.3.2(d)) along the length of the crack. Porosity analysis of the tracks performed using area fraction technique show that the area fraction density of the continuous tracks is found to be greater than 99.5%. Further, a combination of the build rate analysis and porosity analysis is used to select process parameter combination for multiple overlapped track deposition. The multiple overlapped track depositions are analyzed and observed to be defect free in the macro and micro scale.

3.2 Effect of LEPF and interlayer delay period on LDED built Hast-X thin wall structures

One of the exciting applications of LDED is the building of complex shaped thin wall structures with improved material utilization. However, the major issues associated with LDED of thin walls is the deviation in the wall dimensions primarily due to the accumulation of thermal energy leading to temperature rise during continuous layer by layer deposition [24]. Thus, a detailed investigation is carried out to understand the effect of LEPF and interlayer delay on the wall geometry and Hast-X material property. Finite element based numerical simulation tool is deployed to understand the experimental results. For the walls built at different LEPF, it is observed that the variation in wall height increases with an increase in LEPF (see Figure T.3.3(a)) due to relatively higher melt-pool flow at higher LEPF, while the variation in wall width decreases with an increase in LEPF due to reduction in necking phenomenon near the base of the thin wall. The geometry analysis along the build direction shows the maximum deviation for 8.2 kJ/g at lower layers primarily due to necking and presence of partially melted powders, while the maximum deviation for 13.2 kJ/g at the top layer can be due to excessive melt-pool flow. Cellular/ dendritic growth at all conditions using microstructural analysis and a marginal reduction in mechanical properties, i.e., average microhardness (~ 10%), yield strength (~ 3.7%) and ultimate tensile strength (~ 4%) are observed with an increase in LEPF due to reduction in the cooling rate. Numerical simulation shows that the preheat temperature on the previously built layers increases with an increase in LEPF and number of layers.

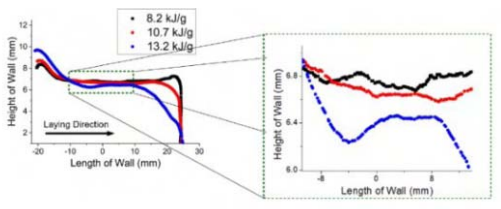

(a)

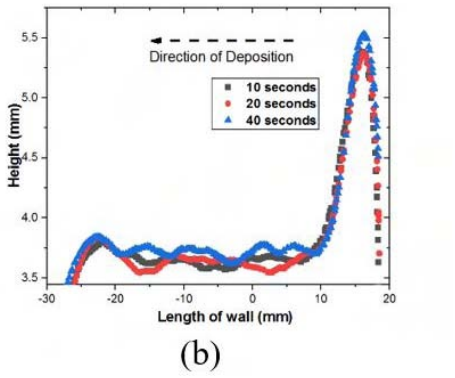

Fig. T.3.3: Effect of (a) LEPF and (b) interlayer delay on wall height.

In case of walls built with different interlayer delay, it is observed that the average wall height is slightly higher for walls built with higher interlayer delay as shown in Figure T.3.3.(b). This is attributed to reduction in preheat temperature (reaching closer to initial temperature) and relatively lower outward flow of the melt-pool with an increase in interlayer delay. The width and variation in wall width decreases with an increase in interlayer delay. Microstructural studies show the presence of cellular and dendritic growth at all conditions with relatively fine grain structure at higher interlayer delay period due to less heat accumulation. The increased interlayer delay yields higher cooling rate and leads to the reduction in elemental segregation along with improved mechanical properties.

3.3 Microstructural and mechanical behavior of LDED built bulk structures

The as-built structures are observed to be defect free in the macro-scale. However, porosity analysis revealed the presence of micro-pores and a relative density of ~ 99.5% is obtained using area fraction technique. The porosity is a mix of circular and irregular pores indicating the presence of gas porosity and lack of fusion porosity, respectively. Optical microscopy and scanning electron microscopy show that the microstructure is a mix of fine cellular and dendritic growth (see Figure T.3.4) and the presence of FCC matrix is revealed during X-ray diffraction studies.

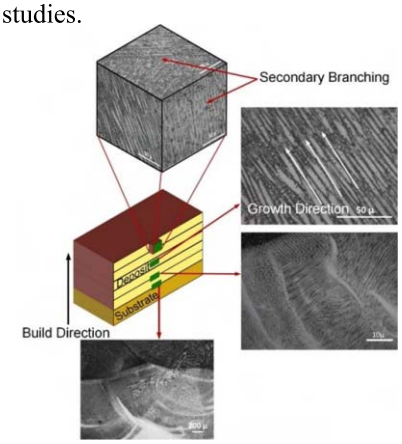

Fig. T.3.4: Microstructure of bulk structures.

The as-built samples revealed random grain orientation with slightly preferred texture along the <100> plane. The elemental mapping revealed the presence of elemental segregations of C, Mo, and Si during the non-equilibrium solidification in LDED. In addition, the presence of Mo rich carbides is also detected, which can be due to the continuous thermal cycling during LDED leading to higher bulk temperature, remelting and carbide formation. Residual stress measurement reveals predominantly tensile stress on the deposited surface with a maximum value of 252 MPa. The measured average micro-hardness is 239 HV1.96N, which is higher than hardness of conventional counterparts (180 HV) [6]. The mechanical properties are analyzed at the room temperature and elevated temperature (up to 600 °C) using automated ball indentation (ABI). The comparison of the mechanical properties at room temperature is presented in Table T.3.1. It is revealed that the yield strength of LDED built Hast-X structures are higher than the conventionally built Hast-X at room temperature and elevated temperature. The higher strength values of LDED built structures can be primarily due to the higher cooling rate resulting in finer grain structure and higher dislocation density in LDED as compared to conventional counterparts. It is also observed that the mechanical strength of bulk structures is higher than that of wall structures built at the same process parameters due to higher cooling rates in bulk structures as compared to wall structures.

Table T.3.1. Comparison of yield strength, ultimate tensile strength and yield ratio for Hast-X through different fabrication routes.

Condition	Yield strength (MPa)	Ultimate strength (MPa)	Yield ratio (MPa)
LDED	478	765	0.62
Conventional [6]	340	760	0.44
LPBF [21]	650	700	0.92

3.4 Effect of in-situ sequential layer-by-layer re-melting (SLLR) and post heat-treatment of Hast-X bulk structures

LDED built Hast-X structures are observed to have lack of fusion porosity, higher surface roughness and non-uniform microstructure. In-situ sequential layer-by-layer laser re-melting (SLLR) and post heat-treatment on the as-built structures are carried out to understand their effect on the properties of LDED built Hast-X. SLLR, a process involving laser re-melting after LDED of each layer, is used to improve the surface and bulk properties of LDED components. SLLR deploys the same laser source used for LDED and scans the laser beam over the previously deposited layer. Initially, single track trials are carried out to select process parameters for bulk deposition. Further, SLLR of bulk structures shows a significant reduction in surface roughness and porosity. Both lack of fusion and gas porosity is observed in the as-built sample, while only gas porosity is witnessed in samples by combining SLLR with LDED. The relative density

increased from 99.5% in as-built samples to 99.99% after SLLR and average surface roughness reduced by 71.4% (Ra from 10.5 µm to 3 µm) after SLLR. Microstructure is found to be relatively fine after SLLR without preferential growth along <100> direction as opposed to that without SLLR due to thermal effect during SLLR. Mo, Si and C segregations and presence of Mo rich carbides are present in LDED and SLLR samples. The finer dendritic microstructures in SLLR samples led to an increase in the microhardness by 12% and yield strength by 7% along the build direction as compared to samples without SLLR.

Further, the microstructure and elevated temperature mechanical properties of Hast-X bulk structures built using LDED is investigated in as-built and post heat-treated conditions. Hast-X, being a solid solution strengthened alloy, solution treatment is carried out at 1177 °C followed by water quenching [6]. Microscopic analysis shows the presence of recrystallized and coarsened equiaxed grains in solution treated samples as opposed to fine cellular and dendritic growth in as-built samples as seen in Figure T.3.5. The solution treated samples revealed random grain orientation as opposed to slightly preferred texture along the <100> plane in the as-built samples. Further, the elemental segregation of Mo, Si and C and precipitation of Mo-rich carbides revealed in the as-built samples are not observed in the solution treated samples. X-ray diffraction studies reveal the presence of nickel γ-matrix and a peak shift is observed after solution treatment, primarily due to change in surface residual stress. The average micro-hardness changed from 239 HV1.96N to 208 HV1.96N after solution treatment, which is similar to microhardness of conventional Hast-X. Single cycle ball indentation studies indicate an increase in energy storage capacity by a factor of 1.55 after solution treatment. ABI tests are used to evaluate the mechanical properties in as-built and solution treated conditions from ambient temperature to 873 K. It is observed that the strength and ABI hardness decreases with an increase in test temperature. The yield strength of solution treated sample is similar to that of conventionally processed wrought Hast-X taken from literature at all test temperatures.

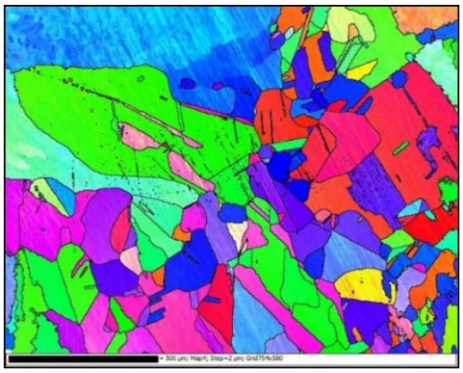

Fig. T.3.5: Microstructure of heat-treated samples.

3.5 Process methodology for LDED of PCHE using wall and bulk structures

PCHE is one of the typical applications of Hast-X in power sector. LDED is attractive for developing PCHEs considering the inherent process advantages. In order to build channels with complex geometries, fabrication of overhang structures is necessary. Overhang walls are deposited using LDED to understand the effect on the angle and uniformity of deposition by varying the process parameters such as percentage overlap (*x*-shift) and a fraction of layer height (*z*-increment), shown in Figure T.3.6 (a). It is observed that when all the other process parameters are kept constant, the maximum *x*-shift that can be deployed for fabricating overhang walls without failure is 15%. When the *x*-shift percentage is above 15%, the wall collapsed after initial few layers. This may be due to the dominance of gravitational force over surface and viscous forces in overhang portion of the wall. The angle made by the wall with the horizontal plane decreases with increased value of *x*-shift for the same *z*-increment. It can also be observed that the angle made by the walls reduces as z-increment decreases. The PCHE is built using a combination of straight walls, overhang walls and bulk structures using the know-how developed from the comprehensive studies as presented in Figure T.3.6(b). LEPF of 10 kJ/g is used for wall deposition and 12 kJ/g is used for bulk deposition. Re-melting of the bulk deposition is also carried out to control surface quality and density. Figure T.3.6(c) presents one of the typical channels built using LDED and Figure T.3.6(d) presents a view of prototype PCHE of size 200 mm x 200 mm x 170 mm built using LDED.

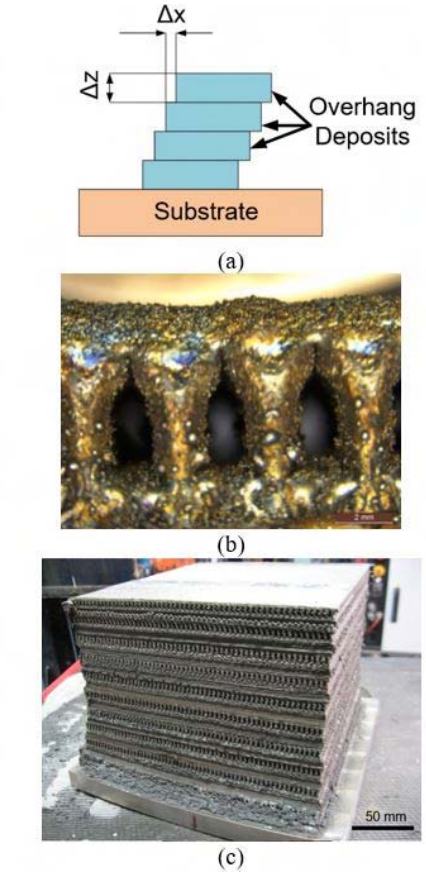

Fig. T.3.6: Overhang wall strategy- (a) schematic, (b) channels and (c) prototype heat exchanger.

4. Conclusions

The present research brings out and contributes to the understanding on the LDED of Hast-X structures from single tracks to multiple overlapped and multi-layer tracks yielding thin walls and bulk structures in terms of processing, geometry, microstructural and mechanical characteristics under different process conditions. It provides insights on to the effect of in-situ treatments and ex-situ post-processing on the behavior of LDED built Hast-X components. The work also contributes to the process methodology development for building PCHEs using LDED.

Acknowledgement

The work presented in this article is part of the Author's Ph.D. thesis work performed under the supervision of Dr. C. P. Paul. The author would like to express immense gratitude to Dr. C. P. Paul. The Author acknowledges the support offered by Dr. S. V. Nakhe, Dr. K. S. Bindra, Dr. Arup Banerjee, members of the Laser Additive Manufacturing Lab at RRCAT, scientific officers at RRCAT for extending testing facilities, and collaborators at VSSC and IGCAR. Author is also thankful for the financial assistance from the Department of Atomic Energy, RRCAT and HBNI, Mumbai.

References

[1] International Organization for Standardization – American Society for Testing and Materials International, ISO/ASTM52900:2015: Additive Manufacturing - General principles - Terminology, 2015.

[2] C. P. Paul, P. Bhargava, A. Kumar, A. K. Pathak, L. M. Kukreja, Laser Rapid Manufacturing: Technology, Applications, Modeling and Future Prospects, J. Paulo Davim (Ed.), Lasers in Manufacturing, UK: ISTE-Wiley, UK, pp. 1-60 (2012).

[3] M. Brandt, Laser Additive Manufacturing: Materials, Design, Technologies, and Applications, 1st ed., Woodhead Publishing, Cambridge, 2016.

[4] M. Brandt, S. Sun, N. Alam, P. Bendeich, A. Bishop, "Laser cladding repair of turbine blades in power plants: from research to commercialization", Int. Heat Treat. Surf. Eng. 3(3), 105 (2009).

[5] M. Perrut, P. Caron, M. Thomas, A. Couret, "High temperature materials for aerospace applications: Ni-based superalloys and γ-TiAl alloys", Comptes Rendus Physique 19 (8), 657 (2018).

[6] Haynes http://www.haynesintl.com/alloys/alloy-portfolio_/High-temperature-Alloys/HASTELLOY-X-alloy/HASTELLOY-X-principal-features.aspx (accessed 29 November 2020).

[7] H. E. McCoy, J. P. Strizak, J. F. King, "Hastelloy-X for High Temperature Gas-Cooled Reactor Applications", Nucl. Technol. 66(1), 161 (1984).

[8] L. Fencheng, L. Xin, Y. Gaolin, S. Menghua, C. Jing, H. Weidong, "Microstructure and residual stress of laser rapid formed Inconel 718 nickel-base superalloy", Opt. & Laser Technol. 43, 208 (2011).

[9] L. Simeng, X. Hui, L. Keyang, X. Wenjia, L. Yanqin, H. Xu, M. Jyoti, S. Lijun, "Melt-pool motion, temperature variation and dendritic morphology of Inconel 718 during pulsed- and continuous-wave laser additive manufacturing: A comparative study", Mater. Des. 119, 351 (2017).

[10] L. Zhichao, L. Tao, N. Fuda, C. Weilong, K. Hoyeol, J. Qiuhong, Z. Hongchao, "Effects of deposition variables on molten pool temperature during laser engineered net shaping of Inconel 718 superalloy", Int. J. Adv. Manuf. Technol. 102, 969 (2019).

[11] C. P. Paul, P. Ganesh, S. K. Mishra, P. Bhargava, J. Negi, A. K. Nath, "Investigating laser rapid manufacturing for Inconel-625 components", Opt. & Laser Technol. 39, 800 (2007).

[12] G. P. Dinda, A. K. Dasgupta, J. Mazumder, "Laser aided direct metal deposition of Inconel 625 superalloy: Microstructural evolution and thermal stability", Mater. Sci. Eng. A. 509, 98 (2009).

[13] F. Makoto, O. Yohei, A. Ryo, T. Kotaro, K. Masaki, "Study on factors for pores and cladding shape in the deposition processes of Inconel 625 by the directed energy deposition (DED) method", CIRP J. Manuf. Sci. Technol. 19, 200 (2017).

[14] B. Guijun, S. Chen-Nan, C. Hui-chi, N. Fern Lan, C. Cho, M. Khin, "Microstructure and tensile properties of superalloy IN100 fabricated by micro-laser aided additive manufacturing", Mater. Des. 60, 401 (2014).

[15] J. O. Milewski, P. G. Dickerson, R. B. Neme, G. K. Lewis, J. C. Fonseca, "Application of a manufacturing model for the optimization of additive processing of Inconel alloy 690", J. Mater. Process Technol. 91, 18 (1999).

[16] A. Ramakrishnan, G. P. Dinda, "Direct laser metal deposition of Inconel 738", Mater. Sci. Eng. A 740-741, 1 (2019).

[17] J. Li, H. M. Wang, "Microstructure and mechanical properties of rapid directionally solidified Ni-base superalloy Rene41 by laser melting deposition manufacturing", Mater. Sci. Eng. A 527, 4823 (2010).

[18] N.I.S. Hussein, J. Segal, D. G. McCartney, I.R. Pashby, "Microstructure formation in Waspaloy multilayer builds following direct metal deposition with laser and wire", Mater Sci. Eng. A 497, 260 (2008).

[19] W. J. Sames, F. A. List, S. Pannala, R. R. Dehoff & S. S. Babu, "The metallurgy and processing science of metal additive manufacturing", Int. Mater. Rev. 61, 315 (2016).

[20] J. N. DuPont, J. C. Lippold, S. D. Kiser, Welding Metallurgy and Weldability of Nickel-Base Alloys, Wiley, Hoboken, New Jersey, 2009.

[21] D. Tomus, Y. Tian, P. A. Rometsch, M. Heilmaier, X. Wu, "Influence of post heat treatments on anisotropy of mechanical behaviour and microstructure of Hastelloy-X parts produced by selective laser melting", Mater. Sci. Eng. A 667, 42 (2016).

[22] M. Pakniat, F. Malek Ghaini, M. J. Torkamany, "Hot cracking in laser welding of Hastelloy X with pulsed Nd:YAG and continuous wave fiber lasers", Mater. Des. 106, 177 (2016).

[23] M. L. Montero-Sistiaga, Z. Liu, L. Bautmans, S. Nardone, G. Ji, J.-P. Kruth, J. V. Humbeeck, K. Vanmeensel, "Effect of temperature on the microstructure and tensile properties of micro-crack free hastelloy-X produced by selective laser melting", Addit. Manuf. 31, 100995 (2020).

[24] Y. S. Lee, D. F. Farson, "Surface tension-powered build dimension control in laser additive manufacturing process", Int. J. Adv. Manuf. Technol. 85, 1035 (2016).